12-2018

Utilizing 3D Printed Analogue Soils to Investigate Specimen Size Effects in Triaxial Testing

Claire Louise Stewart
University of Arkansas, Fayetteville

Utilizing 3D Printed Analogue Soils to Investigate Specimen Size Effects in Triaxial Testing

A thesis submitted in partial fulfillment
of the requirements for the degree of
Master of Science in Civil Engineering

by

Claire Stewart
University of Arkansas
Bachelor of Science in Civil Engineering, 2017

December 2018
University of Arkansas

This thesis is approved for recommendation to the Graduate Council.

Michelle Bernhardt-Barry, Ph.D., P.E.
Thesis Director

Richard Coffman, Ph.D., P.E., P.L.S.
Committee Member

Kevin Hall, Ph.D., P.E.
Committee Member

ABSTRACT

Triaxial testing is one of the fundamental laboratory tests used in geotechnical engineering to determine strength parameters, such as shear strength and friction angle. Investigating the minimum representative elementary volume (REV) can verify the independence of size effects on strength parameters and ensure that the scaled laboratory tests results are consistent, repeatable, and representative of field conditions. Although, REV has been studied for many applications, there is disagreement within geotechnical engineering of a minimum particle diameter to specimen diameter to minimize the size effects related to the REV in consolidated drained (CD) triaxial tests. This research study compared the strength results of three different specimen diameter sizes to understand the size effects and to investigate the influence of particle shape by using 3D printed spheres and scaled Ottawa sand. 3D printed particles allows different influencing variables on strength parameters such as shape, size, gradation, and surface roughness to be controlled within the granular soil. By isolating a factor, such as shape in this case, the response of the soil can be more clearly understood and a representative REV can be determined. The scaled Ottawa sand and spheres had a greater increase in variability as the diameter decreases, implying that the REV was not met for the 7.11 cm specimen diameter. It is recommended that a minimum specimen diameter should be at least nine times greater than the maximum particle diameter for spheres and subrounded particles in consolidated drained triaxial testing in order to minimize size effects.

ACKNOWLEDGEMENTS

I would like to thank my research advisor, Dr. Michelle Bernhardt-Barry, who provided me with guidance, wisdom, and knowledge throughout my research, Bachelor's and Master's degree. Thank you for always having your door open and never being too busy to chat even when you had a million other things to do. I am grateful to have worked with an important role model in my life. I would also like to thank Dr. Richard Coffman and Dr. Kevin Hall for being on my research committee. I would like to thank my mom, my dad, Natalie, Phoebe, and August. I am incredibly humbled by the constant love, encouragement, and support I received throughout this experience. Mom and Dad, thank you for always believing in my capabilities and potential. Natalie, thank you for inspiring me to achieve my goals. Phoebe, thank you for being my number one cheerleader. August, thank you for going on this journey with me and providing patience, comfort, and kind words. Words cannot express my gratitude for everything you all have done for me.

TABLE OF CONTENTS

LIST OF TABLES

LIST OF FIGURES

INTRODUCTION

Triaxial testing is one of the most common geotechnical laboratory element tests to determine strength parameters, but it can give varying results for granular materials due to size effects from failing to fulfill the representative elementary volume (REV) requirement for the test specimen. REV has been described as the smallest material volume element of a composite for which the usual spatially constant 'overall modulus' macroscopic constitutive representation is a sufficiently accurate model to represent a mean constitutive response (Gitman et al., 2006). The REV is not only necessary for geotechnical engineering practice, but for many types of other granular material applications such as the necessary REV in silo flow of different types of grain, granular plant material, and chickpeas (Wiacek et al., 2012, Wiacek and Molenda, 2015). However, there is a lack of research determining size effects caused by REV for coarse-grained soils during consolidated drained (CD) triaxial testing.

This research is comprised of performing CD triaxial testing to investigate the specimen size effects of different specimen diameters with the same particle size and gradation. A gypsum composite was chosen as the 3D printed granular analogue material due to the homogeneity and consistency of the material and so that the REV of different particle shapes could be examined without any changes in material or surface properties. Inherent properties such as gradation, mineralogy, size, surface roughness, and particle shape can be controlled with additive manufacturing technology. Since it is known that particle shape affects the REV, as well as the strength parameters, spheres and scaled Ottawa sand were used to compare the influence of particle shape on the REV and overall soil behavior. Three specimen diameters were tested while the particle gradation was held constant. The specimen size effects were then investigated according to the stress-strain and volumetric responses. Following this introduction, additional

background on REV and specimen size effects is given. Then the methodology for this study is presented, followed by the results, discussion, and conclusions.

BACKGROUND

Since its advent in the 1930's by Dr. Casagrande, triaxial testing has become one of the most prominent geotechnical laboratory element tests for measuring soil shear strength. Its popularity is mainly due to the ease of testing (i.e. setup, controlled drainage, and analysis of the results), and the fact that there are significantly less stress concentrations within the specimen, and unlimited locations of the failure plane (Holtz et al., 2011). Depending on the in situ state of the soil, there are many methods of triaxial tests that can be performed to mimic the actual field conditions. CD triaxial testing was used in this research to replicate a condition of a previously consolidated granular soil with a high permeability, allowing for the drainage of water in the cell volume when an axial load is applied to the soil. Standards have been set which outline the proper testing setup and procedures for CD triaxial testing, so that a soil's shear strength can be accurately predicted; however, the correct particle size to specimen diameter ratios have been a topic of disagreement amongst researchers. Results of CD triaxial testing can be skewed or inconsistent if the largest particle diameter is too large compared to the specimen diameter. Therefore, the REV in CD triaxial testing of granular materials needs to be further investigated.

Representative Element Volume (REV)

All engineering materials that are tested to further understand engineering properties have one important question that needs to be answered before testing begins: what is the volume of material needed (known as REV) which will eliminate size effects? Obtaining the REV when

performing laboratory material tests at a reduced scale is crucial to replicate equivalent results that would be observed in the field. The REV verifies the independence of scaling for the physical and mechanical properties of any type of engineering material. Bear introduced the concept of REV in 1972 with a mathematical concept as presented in Equation 1:

$$n_i \equiv n_i(\Delta U_i) = (\Delta U_v)_i / \Delta U_i \qquad \text{(Equation 1)}$$

where n_i = porosity; ΔU_i = total volume; and $\Delta U_{v_i} =$ the volume of void space. The porosity at a volume much larger than a single grain must be equal to the porosity when gradually reducing the volume: $\Delta U_1 > \Delta U_2 > \Delta U_3 \ldots > \Delta U_i$. Porosity is chosen in this instance as the variable to define the concept of REV, but Bear (1972) also stated that REVs of the medium may need to be defined on the basis of parameters other than porosity, such as stress tensor (Masson and Martinez, 2000), permeability (Ozelim and Cavalcante, 2017), moisture saturation and interfacial area (Costanza-Robinson et al., 2011), and average coordination number (Wiacek and Molenda, 2015.; Masson and Martinez, 2000). Figure 1 represents the scaling effects on porosity as the total volume increases as presented by Bear (1972). The fluctuation of porosity can be seen when a volume is between 0 and ΔU_o due to microscopic effects, when the volume becomes on the order of magnitude of the average distance between the molecules. From ΔU_0 to ΔU_1, the REV is sufficiently captured for homogeneous materials due to the constant porosity value of n. Once the volume reaches ΔU_1 the medium shifts from a homogeneous to inhomogeneous medium, the soil layers are assumed to change.

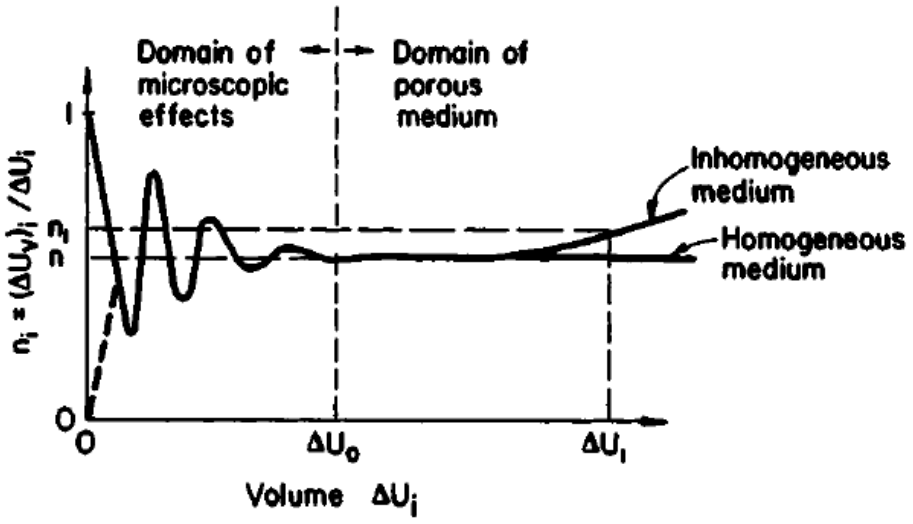

Figure 1: Defining REV in terms of porosity as a function of volume (Bear, 1972).

REV has also been described as the smallest volume of a soil sample where the macroscopic mechanical behavior of the soil can be determined in terms of averages (Wiacek and Molenda, 2015). REV must be determined in order to accurately predict the behavior of materials at different scales (i.e., micro-scale in laboratory testing and macro-scale in the field). Choosing the appropriate test size will dictate the reliability and representation of collected laboratory data. The REV for a certain material is dependent on the material property being studied (Ozelim and Cavalcante 2017; Wiacek and Molenda, 2015). The specimen volume, which ensures macroscale parameters remain consistent over different sizes of the sample, will be different for properties such as permeability and coordination number, which is why it is important to choose the type of limiting boundary condition.

Within granular material related research, theoretical methods (Bear, 1972), physical tests (Holtz and Gibbs, 1956; Razavi et al., 2016; Constanza-Robinson et al., 2011; Wiacek et al., 2012; Omar and Sadrekarimi, 2014, 2015), and numerical tests (Wiacek and Molenda, 2015; Gitman et al., 2005, Ozelim and Cavalcante, 2017) have been conducted in the past to determine

the size effects for different types of granular materials. Meeting the minimum REV has a greater influence on coarse grained materials than fine grained materials, because, typically, granular particle diameters' are orders of magnitude larger than fine grained materials.

REV for Granular Materials

The REV for granular materials is often specified in terms of a specimen diameter to maximum particle size ratio. American Society for Testing and Materials (ASTM) D7181-11 specifies for CD triaxial testing that a specimen diameter must be equal to or greater than six times the largest particle in order to eliminate size effects (ASTM D7181, 2011). This specification is based on Holtz and Gibbs (1956) which determined the specimen to particle diameter ratio for triaxial testing where no size effects were observed on the results. Holtz and Gibbs investigated the relationship between shear resistance and various soil properties (density, amount of gravel, gradation, maximum particle size, and particle shape) during triaxial testing. They were able to compare the shear envelopes of four different sized specimen diameters, 3.50 cm, 8.25 cm, 15.24 cm, and 22.86 cm. The four specimen sizes were used in six conditions in which density, rate of testing, and sand-gravel content were varied. Out of the 16 complete shear tests, the strength results were compared and a marked difference for the stress-strain relationship of the materials was observed. It was determined that the smaller specimen diameters increased in strength as the particle size increased, concluding that the particle diameter of 0.48 cm was too large for the 3.50 cm diameter while the 1.91 cm particle diameter was too large for the 8.25 cm diameter specimen. Holtz and Gibbs determined a maximum particle size for a 15.24 cm diameter specimen was 3.81 cm (4:1 specimen diameter to maximum particle size) and a 22.86 cm diameter test could contain a 7.62 cm particle (3:1 specimen diameter to maximum particle size).

Marachi (1969) specified that a larger specimen diameter to maximum particle size ratio of 6:1 was needed to eliminate size effects.

Other research contradicts the ASTM specifications for the specimen diameter to particle diameter ratios based on size effects. The Eurocode (L.4.1 table L.5 2007), Fagnoul and Bonnechere (1969), and Nitchiporovitch (1969) all specify a minimum sample size to maximum particle size ratio of 5:1 to avoid size effects. Through physical and numerical uniaxial compression testing with adjustable side walls, Wiacek et al. (2012) showed that specimen dimensions greater than five times the mean particle size (as opposed to the maximum) can be used as the REV based on stiffness (Wiacek et al., 2012). The experimental stiffness results of pea grains were compared to similar results from a discrete element method model comprised of spheres to arrive at these findings. Later, Wiacek and Molenda (2015) used discrete element method modeling with spheres and found the minimum specimen diameter needed to be 15 times the mean particle diameter to fulfill the REV in regards to the coordination number, and a REV equal to five and 10 times the mean particle diameter for the elastic modulus and stress ratios, respectively. Masson and Martinez (2000) determined the REVs for different parameters by running DEM simulations comprised of spherical assemblies then comparing the results with analytical and finite element results. The microscopic analysis consisted of determining statistical distribution of contact orientations and contact forces. They found that the specimen size for porosity and coordination number needed to be seven to eight times the largest particle size and that it needed to be 12 times the largest particle size based on the stress tensor. The coordination number in a soil sample is the average number of contacts acting on each particle in the sample (Wiacek and Molenda, 2015).

There have also been several studies which determine the REV for the particle diameter to specimen diameter ratio in terms of porosity. As of recent years, the utilization of x-ray tomography to determine the representative elementary volume based on porosity of granular materials has become a focus (Razavi et al., 2006; Ozelim and Cavalcante, 2017; Borges et al., 2018). Ozelim and Cavalcante (2017) used tomographical reconstructed volumes (Figure 2) and direct scale flow simulations with statistical analysis to conclude that the sand and glass spheres had a REV of 6-10 times the effective diameter, and the clayey sands had a REV of 20-30 times the effective diameter. The effective diameter was a characteristic diameter of the material and defined as 100 divided by the ratio of the summation of percentage fraction of particles between sieves and the mean diameter of particles between two sieves. After the tomographical data was reconstructed, cubic subvolume sampling for evaluation of porosity and permeability were evaluated. The data analysis was repeated for different subvolume sizes which made it possible to analyze how the properties of interest varied according to the change in subvolume sizes.

There has been extensive research in quantifying the REV in soils with porosity as the defining variable, most likely due to Bear's definition of REV with the utilization of porosity. Since the size ratio for triaxial testing is primarily concerned with the strength parameters, it is proposed in this research that REV as function of stress is perhaps a better suited defining factor.

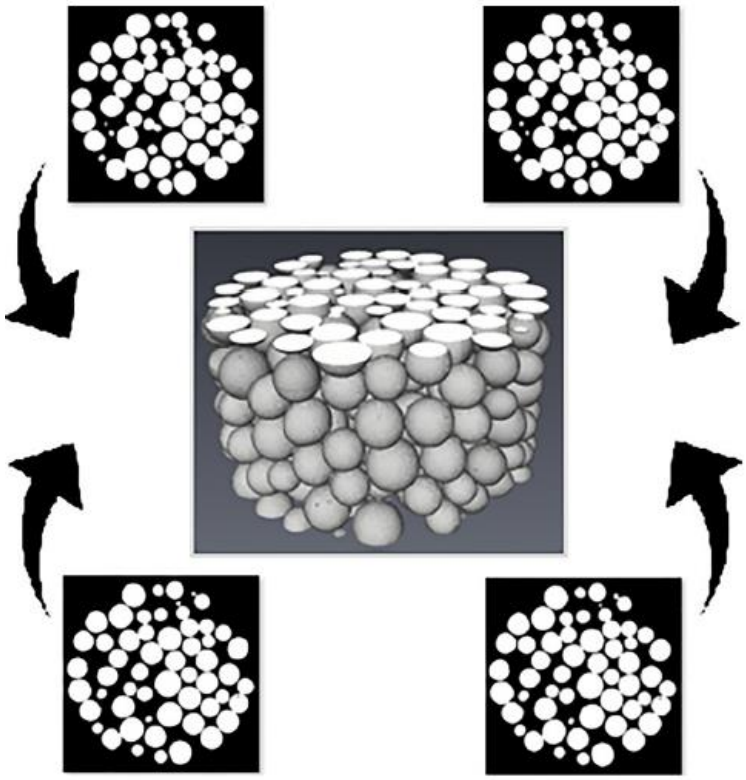

Figure 2: Reconstructed 3D tomographed volumes from 2D slices for REV statistical analysis (Ozelim and Cavalcante 2017).

Quantifying the size effects has also been determined by parameters other than the REV, such as rock and fracture mechanics (Frossard et al., 2012), grain crushing (Marachi, 1969; Marachi et al., 1972, Marsal, 1967, 1972), and maximum grain size effects when the specimen to particle ratio is larger than the mandatory REV (Hu et al., 2011; Omar and Sadrekarimi, 2014, 2015). Grain crushing studies found that particle fracturing increased as the maximum particle size increased, agreeing with the Griffith's crack theory for granular materials (Marachi, 1969). To avoid triaxial testing results with larger friction angles and shear strengths from grain crushing, it has been suggested to have a specimen size no less than 318 times the mean particle diameter or 117 times the maximum particle diameter (Omar and Sadrekarimi, 2014, 2015). On the contrary, other research found that pre-peak behavior of coarse granular materials containing

large particles in triaxial testing is not significantly dependent on the sample size if the REV is met (Hu et al., 2010). Because gravel has comparative large diameter, it is difficult to find triaxial test equipment large enough to minimize size effects. Wei et al. (2010) and Frossard (2006, 2009) investigated whether laboratory tests could be conducted with the same material and gradation, but with smaller size particles with a correlation factor incorporated in the results. This method of testing would also limit grain crushing of gravel.

Particle Shape

While the above studies examined the REV for different factors, the effects of particle shape on REV were not considered. It is a well-known fact that shape of the particles has a significant effect on the strength of the material, i.e. more angular materials have a higher shear strength than more rounded materials (Holtz and Gibbs. 1956; Proctor and Barton 1974; Chan and Page, 1997; Cho et al., 2006; Cavarretta et al., 2010). Different shaped particles also result in varying interparticle force chains within the soil sample which transfer the force from one particle to another in different patterns and change the response of the soil (Parafiniuk et al., 2014). While mineralogy, surface properties, and particle shape affect the strength of a granular material (Bolton, 1986), particle shape was determined to have the greatest effect on macroscopic strength values (Marachi et al., 1972).

The shape of soil particles also influences the REV of a sample (Costanza-Robinson et al., 2011; Razavi et al., 2006; Ozelim and Cavalcante, 2017; Holtz and Gibbs, 1956; Cho et al., 2007; Chan and Page, 1997). Using x-ray computed tomography (CT), Razavi et al. (2006) determined different REVs for spherical, elongated, and subrounded particles by increasing the radius of the 3D particle images. Once soil samples were compacted, the specimen was x-ray scanned to observe the internal structure. With a 3-D interactive image processing program, the

3D images were processed and a REV was chosen as a function of porosity. A computer program was able to determine the three regions of material behavior described by Bear (1972), initial fluctuation region due to microscopic variation, constant region, and region of increase due to heterogeneity (Figure 3). As elongation and angularity increased, the REV increased. It was found that spherical glass beads required a REV of 2-3 times the median diameter of the particle while elongated particles required 5-11 times the median diameter, and Ottawa sand comprised of mainly subrounded particles required a REV of 9-16 times the median diameter.

3D printed gypsum composite spheres and scaled Ottawa sand were chosen for this research due to the effects particle shape has on REV and strength parameters. Although, Razavi et al. (2006) and this research share similar shaped particles of spheres and Ottawa sand, 3D printed particles eliminate any differences in mineralogy and surface properties to allow a comparison of results solely based on particle shape. This research investigates size effects based on the REV using strength as the main determining factor. Determining the correct REV in order to achieve representative soil strengths is important in order to obtain representative values for the design of a number of geotechnical structures.

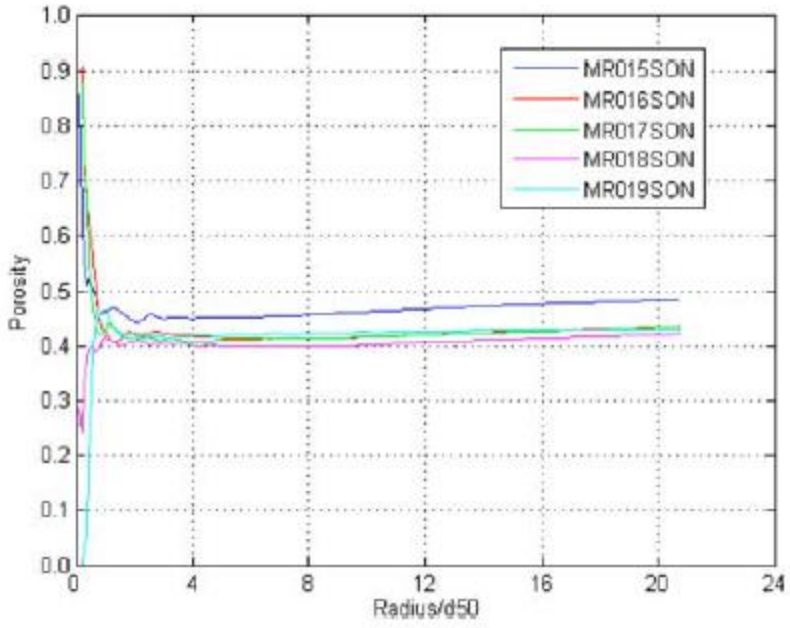

Figure 3: Variation of porosity with normalized radius for Silica sand specimens (Razavi et al., 2006).

METHODOOGY

Material

In this study, 3D printed granular analogue particles were used rather than natural materials due to the homogeneity and consistency of the fabricated material. Natural soils inherently possess internal fracturing, variation in mineralogy, and inconsistent surface properties which can causes difficulties when trying to single out the contribution shape has on the overall behavior. When using additive manufacturing (i.e. 3D printing) to create analogue granular particles, shape can be systematically varied and controlled to determine the influence of the parameter on strength characteristics. Other inherent properties such as gradation, particle size, mineralogy, and surface roughness can also be controlled and held constant while varying particle shapes. 3D printed particles allows for a more accurate investigation of the relationship between individual influencing factors and soil response.

A gypsum composite produced by the Projet 260C device was chosen as the 3D printed analogue soil material for the REV investigation based on findings from Watters and Bernhardt (2017). The soil particles were created out of a powder containing 80-90% calcium sulfate hemihydrate and a binder containing a 2-pyrrolidone. The Projet 260C is a powder bed binder jetting style printer which uses a traditional inkjet cartridge to disperse the binder on the powder. Particles were printed with a 0.1 mm layer thickness and a modified curing process was then followed as seen in Figure 4. The modified curing protocol was implemented to maximize the depth of infiltration of the epoxy which increased the average crushing force by 300% (Watters and Bernhardt, 2017). Two different gypsum composite shapes were printed for this research: scaled Ottawa sand and spheres (Figure 5). Both analogue soil mixtures contained the same gradation with an equal number of particles which had an equivalent diameter of 6 mm, 8 mm, 10 mm, and 12 mm as seen in the gradation curve displayed in Figure 6.

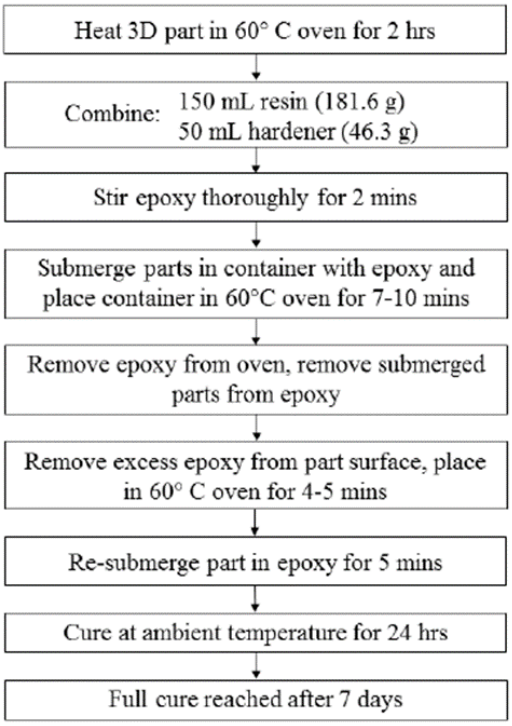

Figure 4: Projet 260C Modified Curing Protocol (Watters and Bernhardt, 2017).

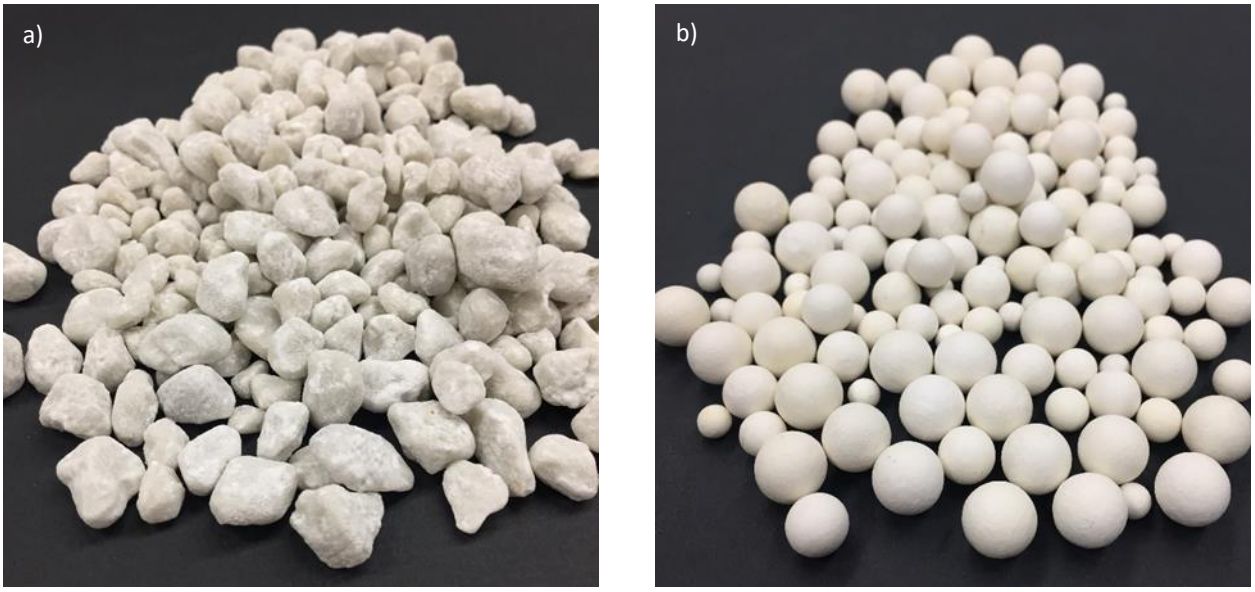

Figure 5: Gypsum composite a) scaled Ottawa sand b) spheres.

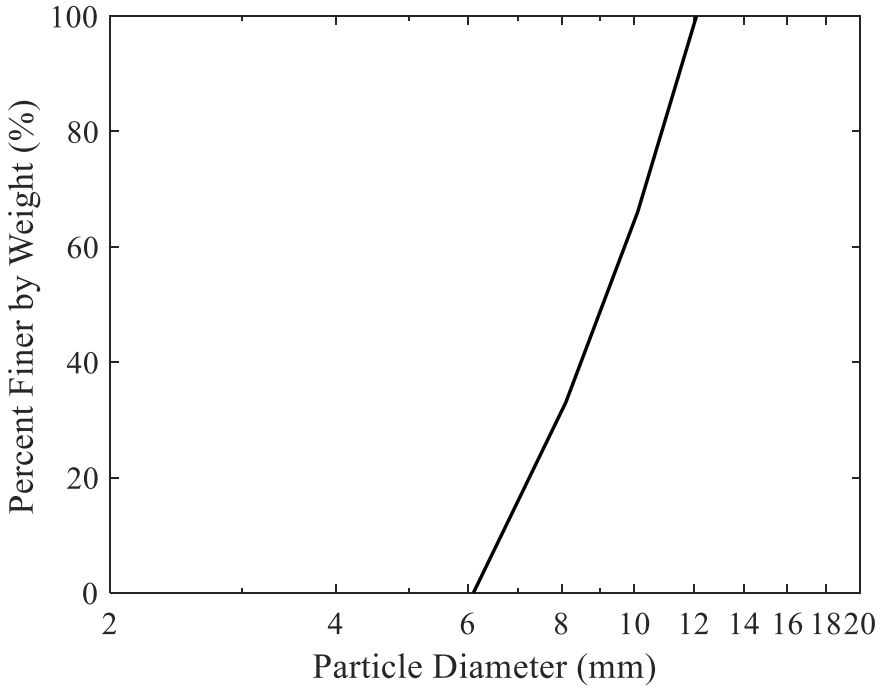

Figure 6: Gradation curve for spheres and scaled Ottawa sand.

The spherical particles were designed in AutoCAD and imported into the 3D Print software as a standard triangular language (STL) file. The scaled Ottawa sand shape was

generated by x-ray computed tomography images of individual grains of Ottawa sand, followed by the determination of volume for each sand particle. The diameter of a sphere with an equivalent volume could then be calculated, then the volume was scaled by a factor resulting in an equivalent volume of 6, 8, 10, 12 mm diameter spheres. This particle size range was chosen for the spheres and scaled Ottawa sand due to the limitations of the Projet 260C printer capabilities and to compare the results of the triaxial tests while maintaining the same gradation and size. Results from extensive material testing of the gypsum composite from Watters and Bernhardt (2017) can be seen in Table 1. In this research, the particle density was calculated for both the scaled Ottawa sand and spheres.

Table 1: Gypsum Composite Material Properties

Scaled Ottawa Sand Grain Density (g/cm^3)	1.55
Sphere Grain Density (g/cm^3)	1.56
Modulus of Elasticity (Gpa)	9.5
Shear Modulus (Gpa)	3.7
Shear Strength (Mpa)	13
Compressive Strength (Mpa)	72.7
Tensile Strength (Mpa)	26.4
Poisson's Ratio	0.3

Set Up

The consolidated drained triaxial tests were performed in accordance to ASTM D7181-11: Standard Test Method for Consolidated Drained Triaxial Compression Test for Soils (ASTM D7181, 2011). Smooth, metal plates with small holes were placed at the end of the specimen to reduce friction and boundary constraints at the end caps while allowing for unrestricted fluid flow. The testing schedule and characteristics of the test specimens can be seen in Table 2. In order to determine the relative density (Dr) of the different test specimens, the minimum and maximum void ratio were determined (Table 2). In order to investigate size effects in CD

triaxial testing, six tests were performed with a large specimen diameter of 15.24 cm, a medium specimen diameter of 10.16 cm specimen diameter, and a small 7.11 cm specimen diameter. The specimen diameter ratio to maximum particle diameter was 13:1 for the large specimen, 9:1 for the medium specimen, and 6:1 for the small specimen. Because these all satisfy the ASTM requirements of 6:1, it could be determined whether this ASTM requirement for particle to specimen diameter sufficiently captures the minimum REV of each specimen and eliminates size effects. For every specimen diameter, three tests were performed with spheres and three scaled Ottawa sand. Samples were densely prepared by using the dry tamping method in five layers with 25 tamps per layer. A 10.16 cm diameter test specimen with scaled Ottawa sand prior to shearing can be seen in Figure 7.

Figure 7: 10.16 cm scaled Ottawa sand specimen prior to shearing.

Originally, ASTM D4253-16 and ASTM D4254-16 were followed to determine the minimum and maximum density of the spheres and scaled Ottawa sand in a metal cylindrical mold with a volume of 3202.71 cm^2 (ASTM D4253, 2016; ASTM D4254, 2016). However, this procedure and mold resulted in unrealistic relative densities for the medium and small specimens as seen in Table 4. The minimum and maximum relative densities were then determined following the same procedures specified in the ASTMs but using the triaxial test split molds (Table 4). The only deviation from the ASTM when determining minimum and maximum density was the size of the mold with the addition of the membrane. The unrealistic relative densities from the ASTM method were most likely due to the influence of specific surface area on the specimen (Table 3). As the specimen diameter decreases, the specific surface area increases resulting in a higher surface area compared to the total volume. When the maximum void ratio (minimum density) was determined, the increase in specific surface area had a significant effect on the number of particles that could fit in the mold by reducing the total amount. The additional friction from the membrane compared to the smooth metal sides of the ASTM mold also influenced the minimum density. The maximum void ratios were similar for the ASTM mold and large triaxial test split mold, because the mold diameters were six inches with different heights. The minimum void ratio (maximum density) was not effected as much by the increase in surface area as the maximum void ratio, but still changed for the spheres and scaled Ottawa sand. The variation in relative density of test samples was most due to the limitations of measurement accuracy. The range of densities tested resulted from differences of less than 2 mm in the sample height and it was very difficult to ensure specimens were inside of this range. The minimum and maximum void ratios determined from the modified procedure rather than the ASTM procedure were used in the data analysis.

Table 2: Test Schedule and Specimen Characteristics

Test Number	Shape	e_{min}, e_{max}	Diameter (cm)	Height (cm)	e	Dr (%)
1	Spheres		15.32	29.58	0.60	89.41
2	Spheres	0.59, 0.76	15.29	29.53	0.61	85.29
3	Spheres		15.32	29.37	0.61	84.12
4	Ottawa		15.29	27.73	0.43	78.36
5	Ottawa	0.36, 0.72	15.28	27.94	0.44	76.99
6	Ottawa		15.28	27.62	0.43	80.82
7	Spheres		10.32	19.21	0.68	72.68
8	Spheres	0.63, 0.83	10.34	19.42	0.68	75.61
9	Spheres		10.36	19.16	0.68	75.12
10	Ottawa		10.34	19.31	0.46	81.80
11	Ottawa	0.39, 0.79	10.30	19.58	0.49	74.42
12	Ottawa		10.34	19.37	0.47	79.83
13	Spheres		7.48	15.40	0.73	69.35
14	Spheres	0.63, 0.95	7.47	15.29	0.73	69.97
15	Spheres		7.47	15.19	0.72	71.52
16	Ottawa		7.50	15.45	0.51	68.54
17	Ottawa	0.37, 0.82	7.49	15.19	0.50	71.40
18	Ottawa		7.53	14.61	0.49	74.04

Table 3: Minimum and Maximum Void Ratio Comparison for Different Molds

Mold Type	ASTM Mold	Large	Medium	Small
Diameter (cm)	15.14	15.36	10.29	7.32
Height (cm)	17.79	30.32	19.56	15.36
Specific Surface (cm^{-1})	0.377	0.331	0.491	0.666
Spheres: e_{min}, e_{max}	0.58, 0.77	0.59, 0.76	0.63, 0.83	0.63, 0.95
Scaled Ottawa: e_{min}, e_{max}	0.35, 0.72	0.36, 0.72	0.39, 0.79	0.37, 0.82

Table 4: Relative Density Comparison of ASTM Mold and Triaxial Test Mold

Diameter (cm)	Shape	Dr (%) with ASTM Mold	Dr (%) with Test Mold
15.32	Spheres	89.11	89.41
15.29	Spheres	85.48	85.29
15.32	Spheres	84.44	84.12
15.29	Ottawa	76.41	78.36
15.28	Ottawa	75.07	76.99
15.28	Ottawa	78.82	80.82
10.32	Spheres	46.58	72.68
10.34	Spheres	49.69	75.61
10.36	Spheres	49.17	75.12
10.34	Ottawa	68.90	81.80
10.30	Ottawa	60.86	74.42
10.34	Ottawa	66.76	79.83
7.48	Spheres	23.76	69.35
7.47	Spheres	24.79	69.97
7.47	Spheres	27.39	71.52
7.50	Ottawa	55.23	68.54
7.49	Ottawa	58.71	71.40
7.53	Ottawa	61.93	74.04

Two sets of triaxial testing equipment including a stand, cap, and acrylic cell were used in this research. The 15.24 cm and 10.16 cm diameter specimen used the larger set of equipment, and the smaller set of equipment was for the 7.11 cm diameter test. Corrections were made for the different equipment sizes regarding frictional force of the piston and the water in the cell displaced from the piston.

The typical setup specified in ASTM D7181 was modified because of a limitation of the gypsum particles (ASTM D7181, 2001). Although they are infiltrated with epoxy, the particles loose strength significantly if they are submerged in water for long periods of time (Watters and Bernhardt, 2017). To avoid this, water was not used within the pore space and instead, a pressure panel supplied air pressure to maintain the pore pressure of the specimen. The cell pressure was

generated by fluid pressure using de-aired water as in the traditional setup. Due to the large volume of water moving in and out of the cell during shearing, a custom bladder system was used to regulate the cell pressure surrounding the soil specimen and measure the change in volume of the specimen (Figure 8). The average volume of water displaced during the 15.24 cm test was 416 cm^3 which is much larger than typical flow pump volume systems available. The bladder system is comprised of a rubber bladder fixed inside an acrylic cell containing water which is placed on a load cell to monitor the volume change within the cell. Air pressure supplied by a panel is used to regulate the air pressure inside of the bladder, and the rubber bladder can be inflated to displace water surrounding the bladder and increase the pressure or deflated to decrease the pressure. As the dense samples underwent shearing they dilated which displaced water from the surrounding cell into the water pressure bladder system. This resulted in an increase in the load measured for the cell and thus, the volume change could be monitored accordingly.

Backpressure saturation occurred over a time span of 24 hours to dissolve any remaining air into solution. A pore pressure Parameter B to determine complete saturation was not calculated due to the use of pore air pressure, but instead saturation was determined when the change in water load as a function of time approached zero. During backpressure saturation and shearing, the cell pressure was 344.7 kPa, and pore pressure was 244.7 kPa, resulting in an effective confining stress of 100 kPa. Preliminary tests with pore water pressure and pore air pressure were performed to verify to ensure that the modified procedures resulted in the same response. These tests and the verification are further described in the Results and Discussion section.

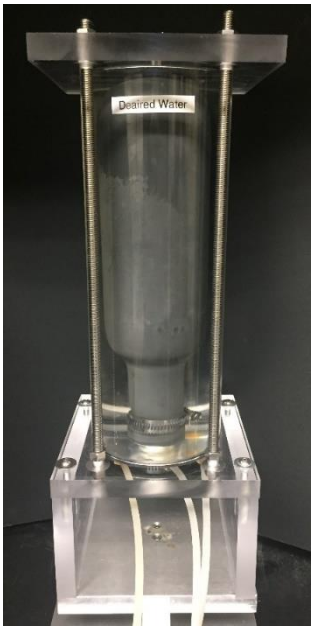

Figure 8: Bladder system supplying water to triaxial test cell volume.

A consolidation test (ASTM D2435, 2011) was performed on a 15.24 cm test specimen comprised of the gypsum composite spheres to determine a maximum shear rate of 0.366 %/min according to ASTM D7181-11 (ASTM D7181, 2011). In order to ensure the shear rates for the test specimen were below the maximum shear rate and no excess pore water pressure occurred during shearing, the rate was set at 0.0177 in/min. This resulted in 0.003%/min for the large specimen (122 times slower than the maximum shear rate), 0.004%/min for the medium specimen (92 times slower than the maximum shear rate), and 0.006%/min for the small specimen (61 times slower than the maximum shear rate). All tests were conducted until the axial strain reached 15%, but at approximately 13% axial strain, the 15.24 cm test specimens bulged in the middle of the specimens and contacted the acrylic cell. These tests were stopped once contact was made.

A number of monitoring instruments were incorporated in the triaxial testing including an Omega PX409-150GV pore pressure transducer, an Omega PX409-150GV cell pressure transducer, an Omega HSTC-TT-J-24S-36 thermocouple, an Interface SSM-AJ-5000 load cell

measuring the applied load, a HBM SP4MC6MR load cell measuring the change in water volume in the bladder system, and an Omega LDI-119-075-A010A linear variable inductance transducer (LVIT) measuring the displacement of the piston. The code for instrument calibrations, reading and displaying data on a continuous time graph, and recording the information was written in the National Instrument's computer program *LabVIEW*. *LabVIEW* recorded and averaged 10 reading per second for each device. The time, cell pressure, pore pressure, temperature, applied load, change in water load, and piston displacement were recorded in engineering units every second in *Excel* as well as the mass, diameter, and height of the sample. The data analysis was then performed in *MATLAB*. A schematic of the consolidated drained triaxial test setup can be seen in Figure 9.

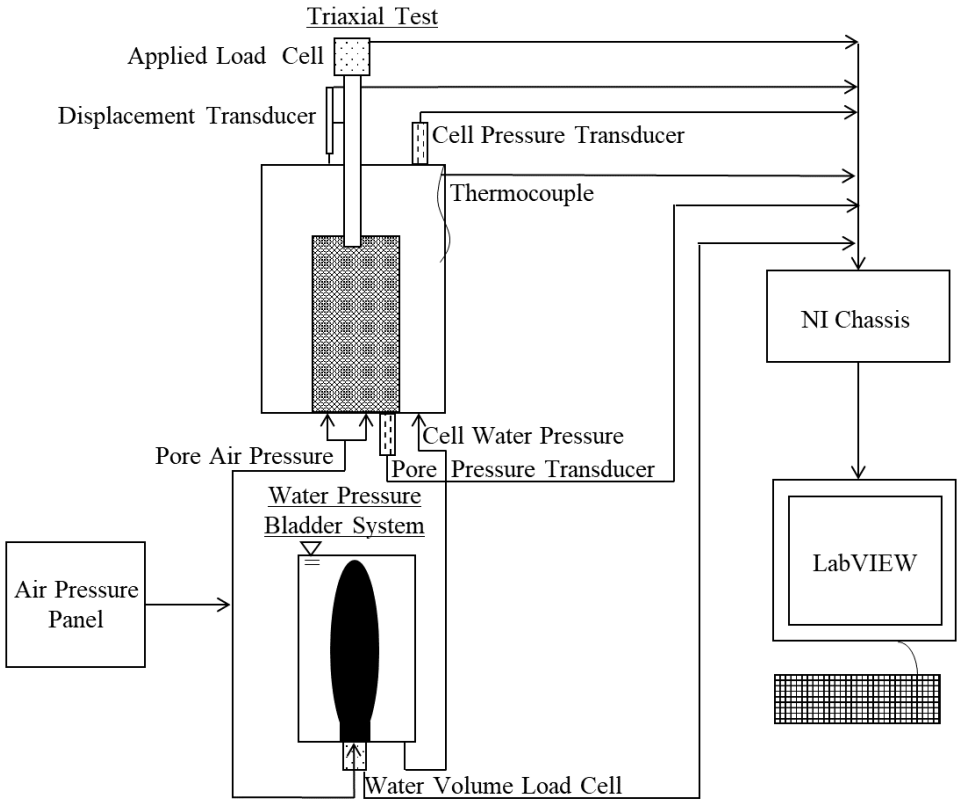

Figure 9: Triaxial test setup schematic.

RESULTS AND DISCUSSION

Corrections

Several correction calculations were incorporated into the results. Corrections were made for membrane penetration of the sample, temperature of water, membrane strength resistance, the change in cross sectional area during shearing, the frictional force related to the piston movement through the cell top cap, and the volume of water displaced by the piston. The membrane penetration of the soil sample affects the volumetric strain in drained tests (Baldi and Nova, 1984). One of the most important factors of membrane penetration is the size of the particle, and since this research uses particles up to 12 mm in diameter, it is mandatory to correct for this issue (Baldi and Nova, 1984; Frydman et al., 1973; Steinbach, 1967). The change in cell water volume due to membrane penetration is dependent on confining pressure, rigidity, and thickness of the membrane. The common simplified equation for membrane penetration created by Baldi and Nova is not used for this research, because it assumes a very small particle diameter (≤0.5 mm) which may lead to appreciable errors (Baldi and Nova, 1984). A more accurate membrane penetration correction when using particles with mean particle diameter of 9 mm (Equation 2) was applied:

$$V_m = \frac{1}{2}\frac{\sigma_3 d_g}{E_m t_m}\frac{d_g}{D}\left(\frac{V_o}{sin^2\left(\left(\frac{\sigma_3 d_g}{E_m t_m}\right)^{\frac{1}{3}}\right)}\right) \qquad \text{Equation 2}$$

The confining stress, σ_3, initial volume of the sample V_o, and diameter of the sample D were determined at the time of the triaxial test. The thickness of the membrane, t_m, for the tests was 1.168 mm. Young's Modulus of the latex membrane, E_m, was determined by Welcher (2004) to

be 1815kPa. The mean grain diameter, d_g, (a representative size of the granular material) was 9 cm. (Baldi and Nova, 1984). The volume of membrane penetration was used to determine the corrected initial sample volume.

A temperature correction for the unit weight of water was necessary when determining the volumetric strain of the specimen. As temperature increases, water has greater energy, and the density of water of water decreases. Equation 3 was used to determine the density of air free water according to Jones and Harris (1992).

$$\rho = 999.85308 + 6.32693 * 10^{-2}t - 8.523829 * 10^{-3}t^2 + 6.943248 * 10^{-5}t^3 \ldots$$
$$-3.821216 * 10^{-7}t^4 \qquad \text{Equation 3}$$

This equation, an adaptation from Kell (1975), was fitted over the 1990 International Temperature Scale (ITS-90) temperature range of 5-40°C. The temperature, *t*, was recorded in degrees Celsius. ASTM D7181-11 provided a correction for the additional strength of the membrane resistance affecting the principal stress difference as seen in Equation 4 (ASTM D7181,2011).

$$\Delta(\sigma_1 - \sigma_3) = \frac{4E_M t_m \varepsilon_1}{D_c} \qquad \text{Equation 4}$$

Similar to Equation 2, the Young's Modulus of the membrane was 1815 kPa, and the thickness of the membrane was 1.168 mm.

Rather than using the corrected area equation in ASTM D7181-11 which assumes deformation as a right circular cylinder during shear, an area correction was incorporated assuming a vertically parabolic shaped failure (ASTM D7181, 2011). A parabolic shaped failure is a more appropriate assumption for this research due to the significant bulging during shearing. Originating from Zhang and Garga (1997), the corrected area can be seen in Equation 5.

$$A_e = A_c\left(-0.25 + \frac{\sqrt{(25-20\varepsilon_a-5{\varepsilon_a}^2)}}{4(1-\varepsilon_a)}\right)^2 \qquad \text{Equation 5}$$

The corrected area, A_e, was computed at the mid-height of the specimen where the maximum specimen diameter occurred (Zhang and Garga, 1997). Equation 5 was a function of the cross sectional area before shearing, A_c, and axial strain, ε_a.

The frictional force associated with the piston and the displacement of cell water from the piston were determined for both the smaller and larger set of triaxial equipment for data. The frictional force was determined by measuring the force associated with the piston movement before contact was made with the specimen. This value was subtracted from the load measured during shearing. The volume of water displaced by the piston was calculated by multiplying the displacement of the piston by the cross sectional area of the piston. The displacement of water from the piston was subtracted from the total change in cell water volume.

A verification of using pore air pressure rather than pore water pressure can be seen in Figure 10. Figure 10.a. and 10.b. represent the triaxial test results before the corrections were applied, and Figure 10.c. and 10.d. represent the results when the corrections are incorporated in the data analysis. The results of two consolidated drained triaxial tests can be seen where one test with pore water pressure is represented in blue and one test with pore air pressure is represented in red. The two tests were performed with the same strain rate and confining pressures as the 18 tests with the gypsum composite. Spheres created from a photopolymer material with the same gradation and size as the tests with the gypsum composite were used for the verification tests. After the corrections are applied, the change in pore volume and cell volume when using pore water pressure and the change in cell volume when using pore air pressure are in good agreement (Figure 10.c.). The similarity of the change in water volume when comparing the two tests

results in rate of dilation, represented by the volumetric strain, that is in good agreement. Figure 10 also verifies the repeatability of the testing method by displaying the results of two separate tests that are very similar.

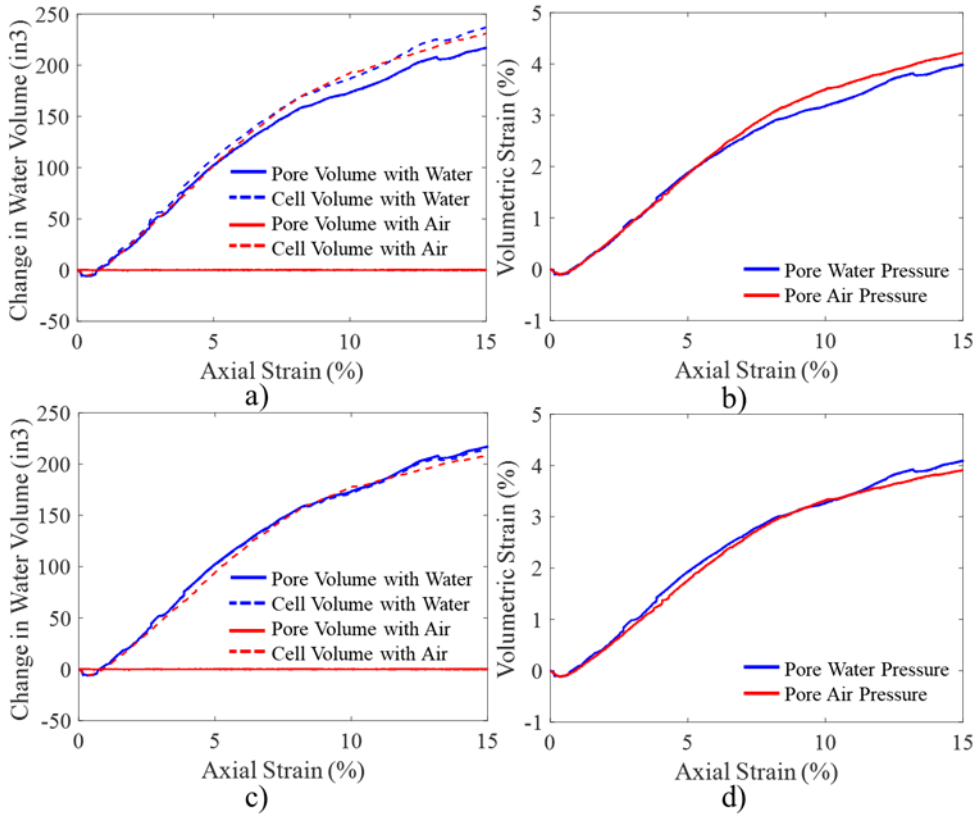

Figure 10: Comparison of pore air pressure and pore cell pressure: a) uncorrected volumetric strain b) uncorrected change in water volume c) corrected volumetric strain d) corrected change in water volume.

Shearing Results

The testing results were grouped into five sections: spheres, scaled Ottawa sand, small diameter specimen, medium diameter specimen, and large diameter specimen. The triaxial shearing results for the nine spheres tests with the large, medium and small diameters can be seen in Figure 11. The principal stress difference as a function of axial strain for the specimens comprised of spheres can be seen in Figure 11.a. Generally, the stress-strain curves for all the spheres reach a

peak principal stress difference followed by gradual strain softening. The sporadic drops in principal stress difference are most likely due to the interparticle force chains collapsing and rearranging. This is a common occurrence observed in discrete element simulations of spheres. It is clear that these collapses are more frequent and pronounced for the small diameter specimen. The variability in peak principal stress difference for the small specimen diameter is also greater.

All the tests display dilative behavior as axial strain increases which is expected due to the densely prepared samples and rather low confining stress (Figure 11.b.). As the specimen diameter decreases, the total volumetric strain decreases and sudden drops in volumetric strain can be observed. These sudden drops are related to the force chain collapse and rearrangement of the particles, and it is clear that this has more of an effect on the overall response for the small diameter specimens. It is noted that the relative density is lower for these specimens which corresponds with less dilation. Therefore, less dilation in this case may be more associated with density rather than any specimen size effects. The variability in the volumetric and stress responses; however, are likely due to the specimen size effects. The range of densities is much less for these specimens, although the results have a considerable amount of variability when compared to the results from the large specimen which had a larger density range.

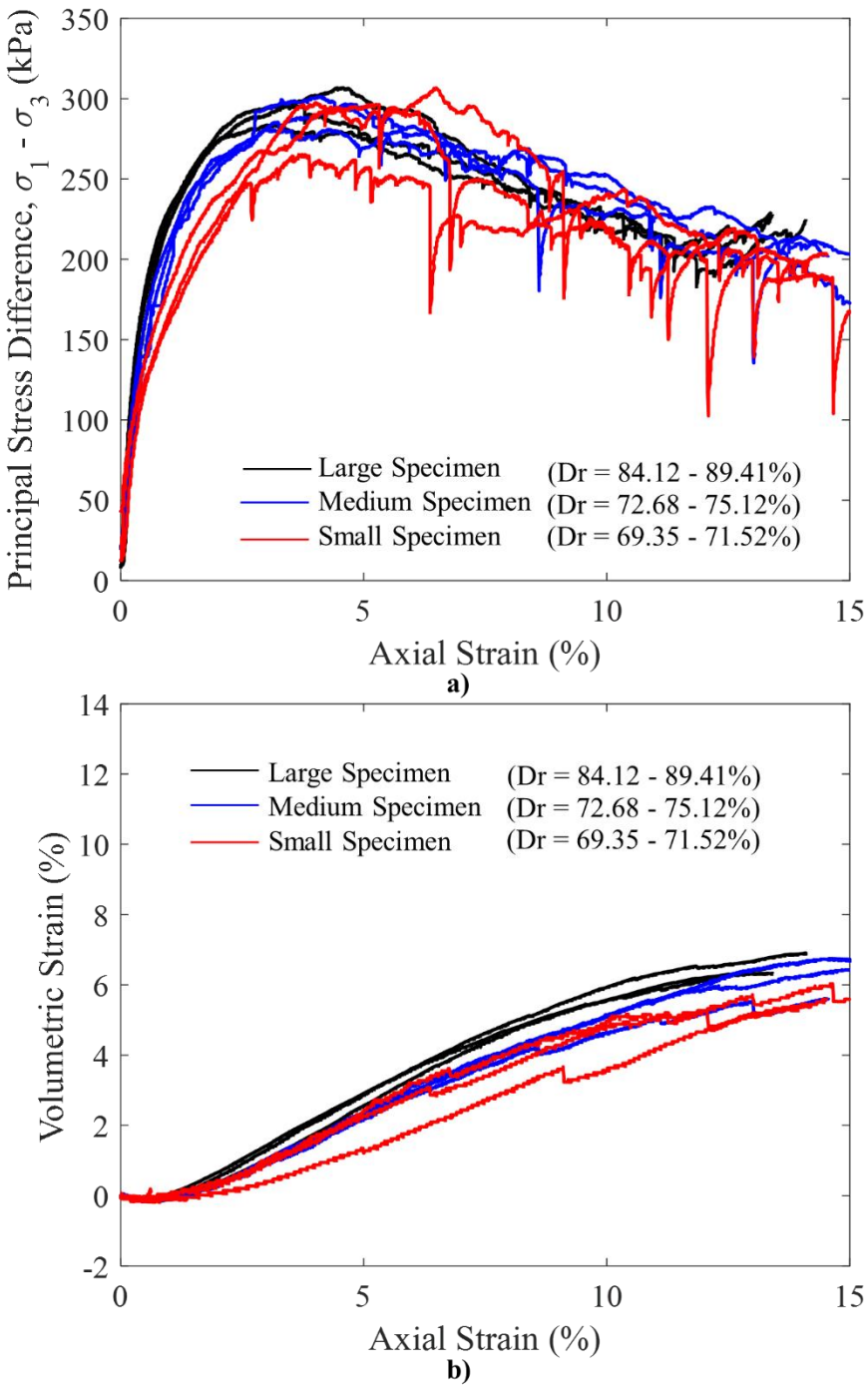

Figure 11: Triaxial shear behavior of spheres with large (15.24 cm diameter), medium (10.16 cm diameter), and small (7.11 cm diameter) specimen: a) principal stress difference b) volumetric strain.

The Mohr's circles for the nine tests on spheres can been found in Figure 12. The minor principal stress of 100 kPa is uniform throughout the test due to the consistent confining pressure, while the major principal stress is more variable, ranging from 366.11 kPa to 410.76 kPa. The failure envelope is displayed with the assumption that there is no cohesion in the granular material. The friction angle ranges from 34.61 – 37.18 °. The relative density, principal stress difference at failure, maximum obliquity at failure, axial strain at failure and friction angle for each test can be found in Table 5. While there are no large differences in the friction angles obtained for the three specimen diameters, the range of friction angles obtained is greatest for the small specimen. The range in friction angle of 2.57 ° is likely negligible for most geotechnical problems, however. It is also noted that one would expect the friction angles to be lower for the small specimen because of the lower density; however, it resulted in the highest friction angle. Therefore, the results suggests that the REV was met for the nine tests on spheres due to the narrow range of strength results; however, it is likely that the small specimen may slightly violate the suitable REV. It is recommended that the larger specimen sizes be used in future tests.

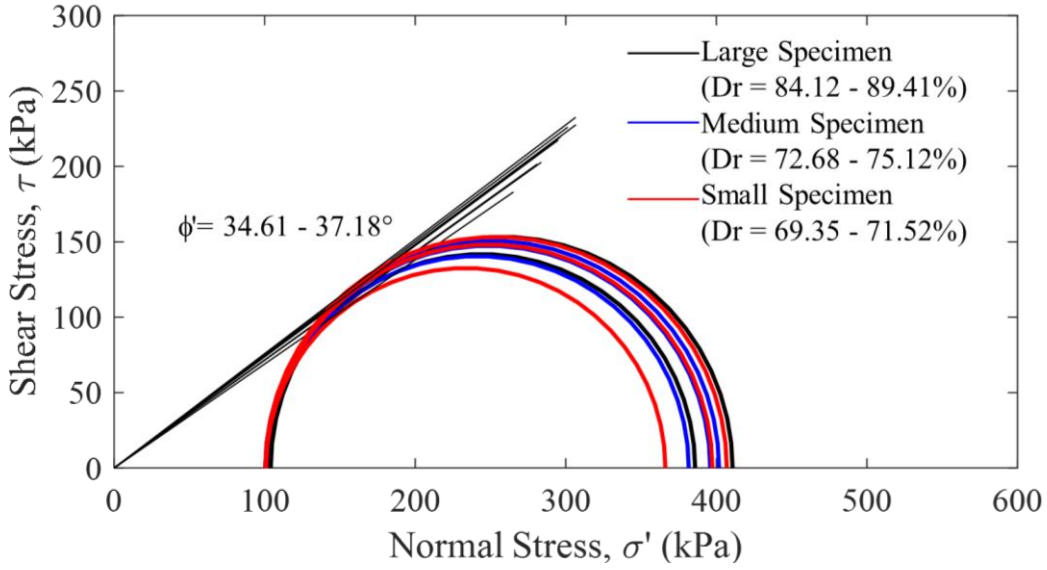

Figure 12: Mohr's Circle for spheres with large (15.24 cm diameter), medium (10.16 cm diameter), and small (7.11 cm diameter) specimen with friction angle range.

Table 5: Test Results for Spheres

D (cm)	Dr (%)	$\sigma'_{1,f} - \sigma'_{3,f}$ (kPa)	$\sigma'_{1,f}/\sigma'_{3,f}$	$\varepsilon_{a,f}$ (%)	ϕ'(°)	$\phi'_{max} - \phi'_{min}$ (°)
15.32	89.41	306.76	3.95	4.58	36.58	
15.29	85.29	283.75	3.78	3.15	35.55	1.03
15.32	84.12	295.60	3.94	3.42	36.52	
10.32	72.68	294.92	3.92	4.56	36.40	
10.34	75.61	281.04	3.79	3.01	35.65	1.23
10.36	75.12	301.35	4.00	4.10	36.88	
7.48	69.35	265.25	3.63	3.79	34.61	
7.47	69.97	306.58	4.06	6.49	37.18	2.57
7.47	71.52	296.54	3.94	5.25	36.53	
Average	77.01	292.42	3.89	4.26	36.21	1.61
Standard Deviation	6.96	12.75	0.12	1.05	0.75	0.68

The results for the scaled Ottawa sand can be found in Figures 13 and 14. Figure 13 displays the triaxial shear behavior of scaled Ottawa sand with 15.24 cm diameter, 10.16 cm diameter, and 7.11 cm diameter specimens. As expected, the stress at failure for the Ottawa sand is higher than the stress at failure for spheres followed by a faster rate of strain softening as seen in Figure 13.a. As the specimen diameter decreases, the maximum principal stress difference becomes more variable, i.e., the small specimen has the largest and one of the smallest peak principal stress differences at failure. The large variation in stress-strain response indicates imposed size effects on the small specimen.

Like the spherical particles, the scaled Ottawa sand dilates during shearing (Figure 13.b). The total volumetric strain is larger for the scaled Ottawa sand than for the spheres which aligns with the higher peak strengths. There are fewer drops in volumetric strain for scaled Ottawa sand than for spheres which is most likely due to greater interlocking forces from the particle shape.

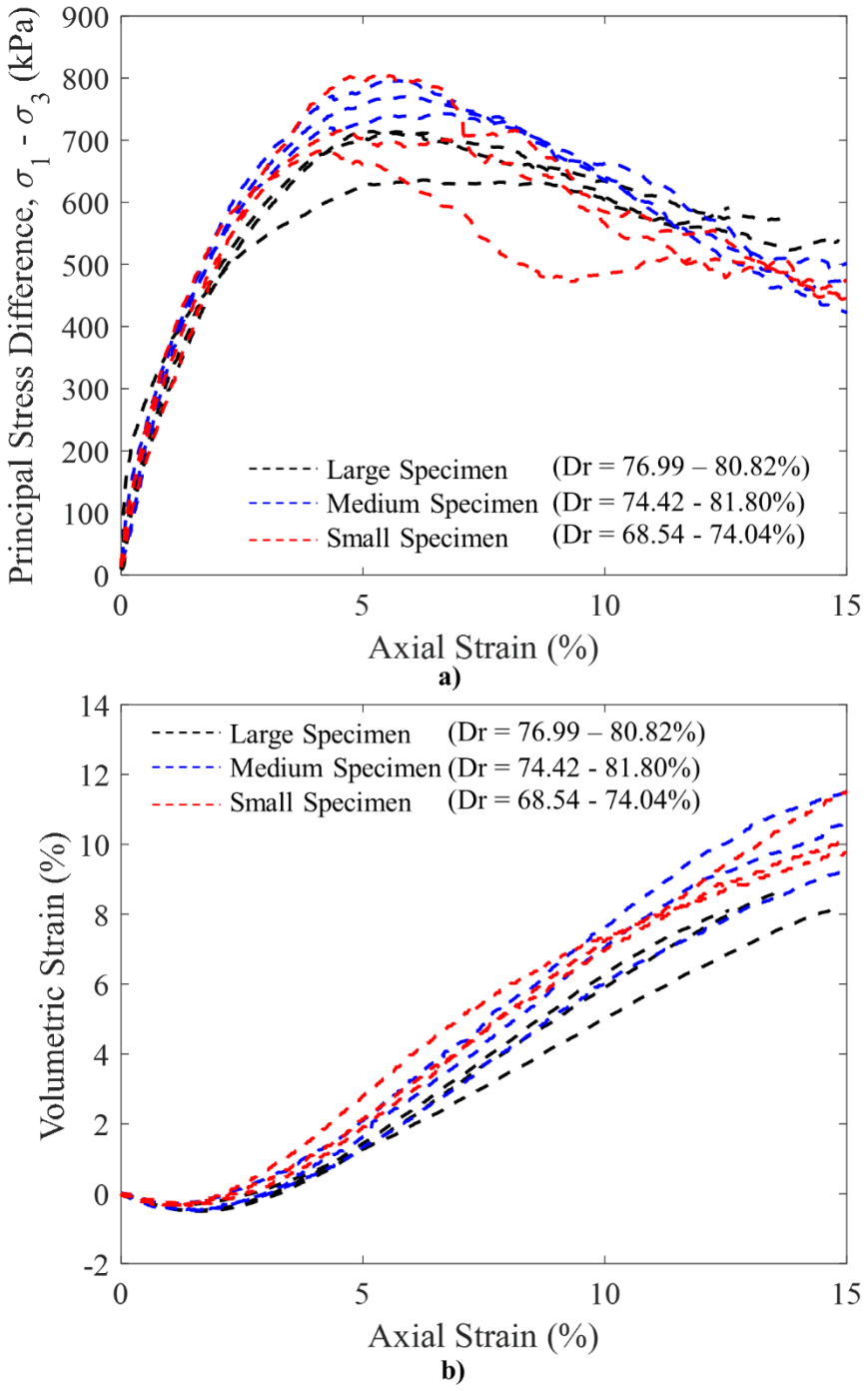

Figure 13: Triaxial shear behavior of scaled Ottawa sand with large (15.24 cm diameter), medium (10.16 cm diameter), and small (7.11 cm diameter) specimen: a) principal stress difference b) volumetric strain.

Mohr's circle for the scaled Ottawa sand with the failure envelope and friction angle can be found in Figure 14. The friction angle ranges from 49.46 - 53.11°. The small specimen had a friction angle range 2.5°, at least twice the range as the medium and large specimen. The 3.65° friction angle difference is negligible in geotechnical engineering practice. Similar to the spheres, the small specimen resulted in the highest friction angle even though the relative density was lower. The high strength of the medium specimen coincides with the large amount of dilation and peak principle stress difference while the erratic soil response of the 7.11 cm tests is clearly reflected by the range of locations for the major principal stress from 783.49 kPa to 905.82 kPa. The results for scaled Ottawa sand can be found in Table 6. The standard deviation of the principal stress difference is larger for the scaled Ottawa sand than the spheres, implying that there was greater variability in results for the three specimen sizes. The variability in friction angle and principle stress difference for the 7.11 cm diameter indicates the REV was not met for the scaled Ottawa sand.

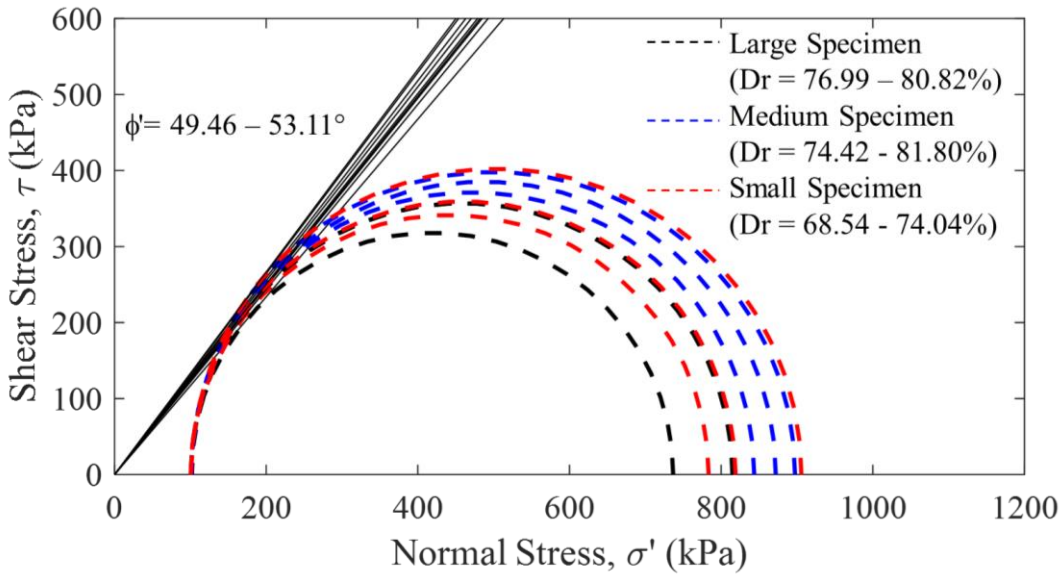

Figure 14: Mohr's Circle for scaled Ottawa sand with large (15.24 cm diameter), medium (10.16 cm diameter), and small (7.11 cm diameter) specimen with friction angle range.

Table 6: Test Results for Scaled Ottawa Sand

D (cm)	Dr (%)	$\sigma'_{1,f} - \sigma'_{3,f}$ (kPa)	$\sigma'_{1,f} / \sigma'_{3,f}$	$\varepsilon_{a,f}$ (%)	ϕ (°)	$\phi_{max} - \phi_{min}$ (°)
15.29	78.36	714.33	8.00	5.20	51.07	
15.28	76.99	636.20	7.33	6.24	49.46	1.75
15.28	80.82	713.92	8.07	5.66	51.21	
10.34	81.80	796.32	8.88	5.73	52.90	
10.30	74.42	742.95	8.39	6.62	51.90	1.00
10.34	79.83	770.55	8.59	5.88	52.33	
7.50	68.54	683.09	7.80	4.14	50.61	
7.49	71.40	718.63	8.16	4.62	51.41	2.50
7.53	74.04	805.06	8.99	5.55	53.11	
Average	76.24	731.23	8.25	5.52	51.56	1.75
Standard Deviation	4.23	51.06	0.50	0.72	1.09	0.61

A comparison of spheres and scaled Ottawa sand with large, medium and small specimen sizes can be seen in Figures 15-18. The impact on strength parameters from particle shape becomes apparent when comparing the spheres and scaled Ottawa sand on the same figure. Since the gradation, size, and mineralogy are the same for the tests, the difference in maximum principal stress difference and friction angle is due to the impact of spherical and subrounded particles for each specimen diameter. Figures 15.a., 16.a., and 17.a. display the principal effective stress as a function of axial strain for the spheres and scaled Ottawa sand with a 15.24 cm, 10.16 cm, and 7.11 cm specimen diameter, respectively. When plotting spheres and scaled Ottawa sand on one figure, the difference in strain-softening can be differentiated. Scaled Ottawa sand had a faster rate of strain softening than the spheres. The scaled Ottawa sand has a much higher principal stress difference at failure and distinct peak. As the specimen diameter decreases, the differences in the results observed for the spheres and Ottawa sand increase. The results for the spheres appear to remain more consistent than the scale Ottawa sand for the different specimen sizes, as shown by the similar principal stress differences at failure as well as

the principal stress difference curves. The 10.16 cm specimen displays a higher rate of strain softening for scaled Ottawa sand compared to the 15.24 cm specimen. The small specimen has the greatest amount of variability of principal stress difference for both the spheres and scaled Ottawa sand. After the peak principal stress difference, the strain softening no longer follows a linear trend as seen for the medium and large specimen.

Figure 15.b., Figure 16.b., and Figure 17.b. display the volumetric strain as a function of axial strain for scaled Ottawa sand and spheres with a 15.24 cm, 10.16 cm, and 7.11 cm specimen diameter, respectively. All tests resulted in a dilative response to shearing. The relationship between volumetric strain and axial strain is most similar for the 15.24 cm for the spheres and scaled Ottawa sand when compared to the medium specimen and small specimen. As the test diameter decrease, the difference dilation between the scaled Ottawa sand and spheres increases. The change in specimen volume for the scaled Ottawa sand is higher than for spheres for every test specimen size. The frequency of sudden drops in volumetric strain for spheres due to particle force chains collapsing and rearranging increases as the diameter decreases.

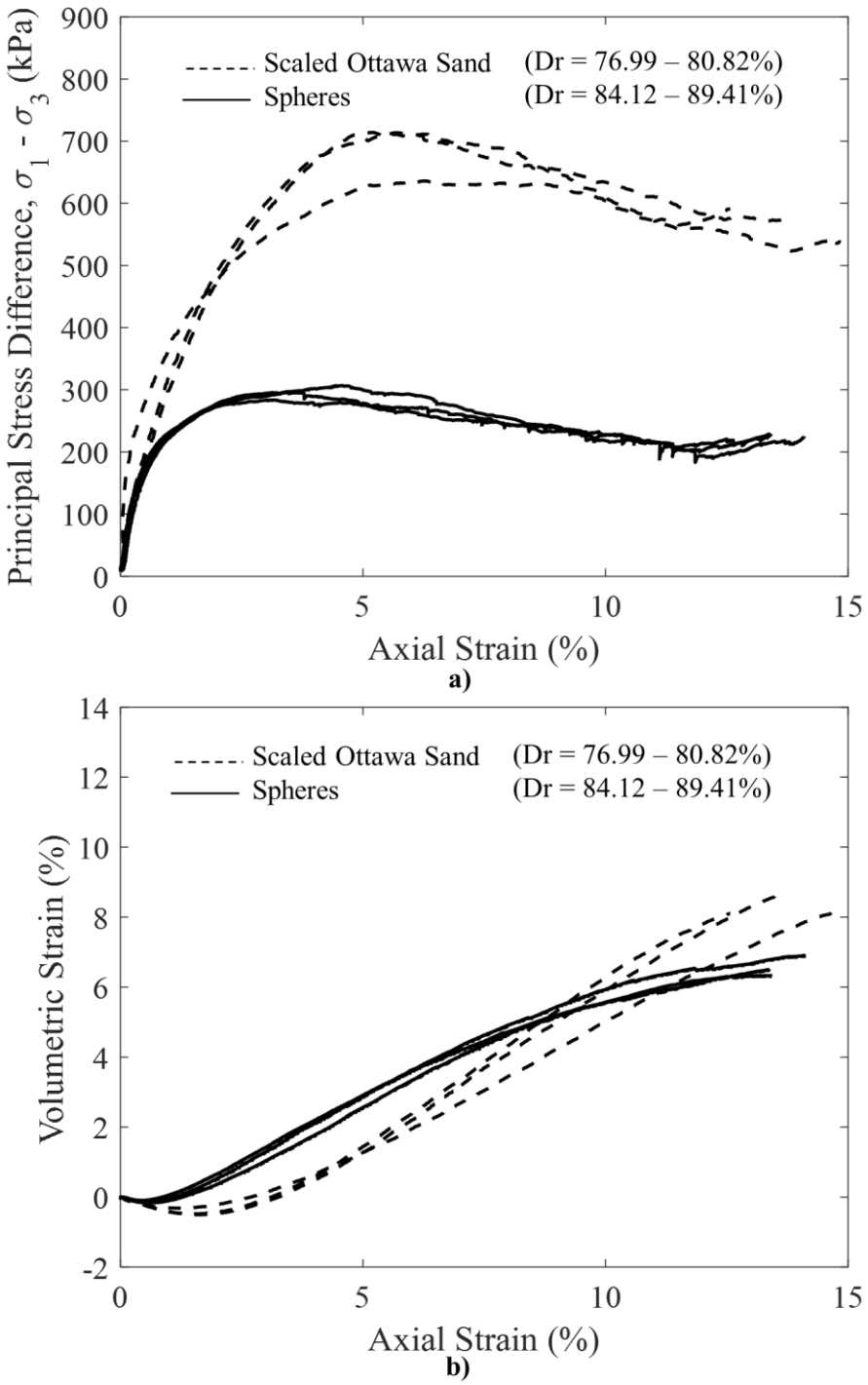

Figure 15: Triaxial shear behavior of scaled Ottawa sand and spheres with large (15.24 cm diameter): a) principal stress difference b) volumetric strain.

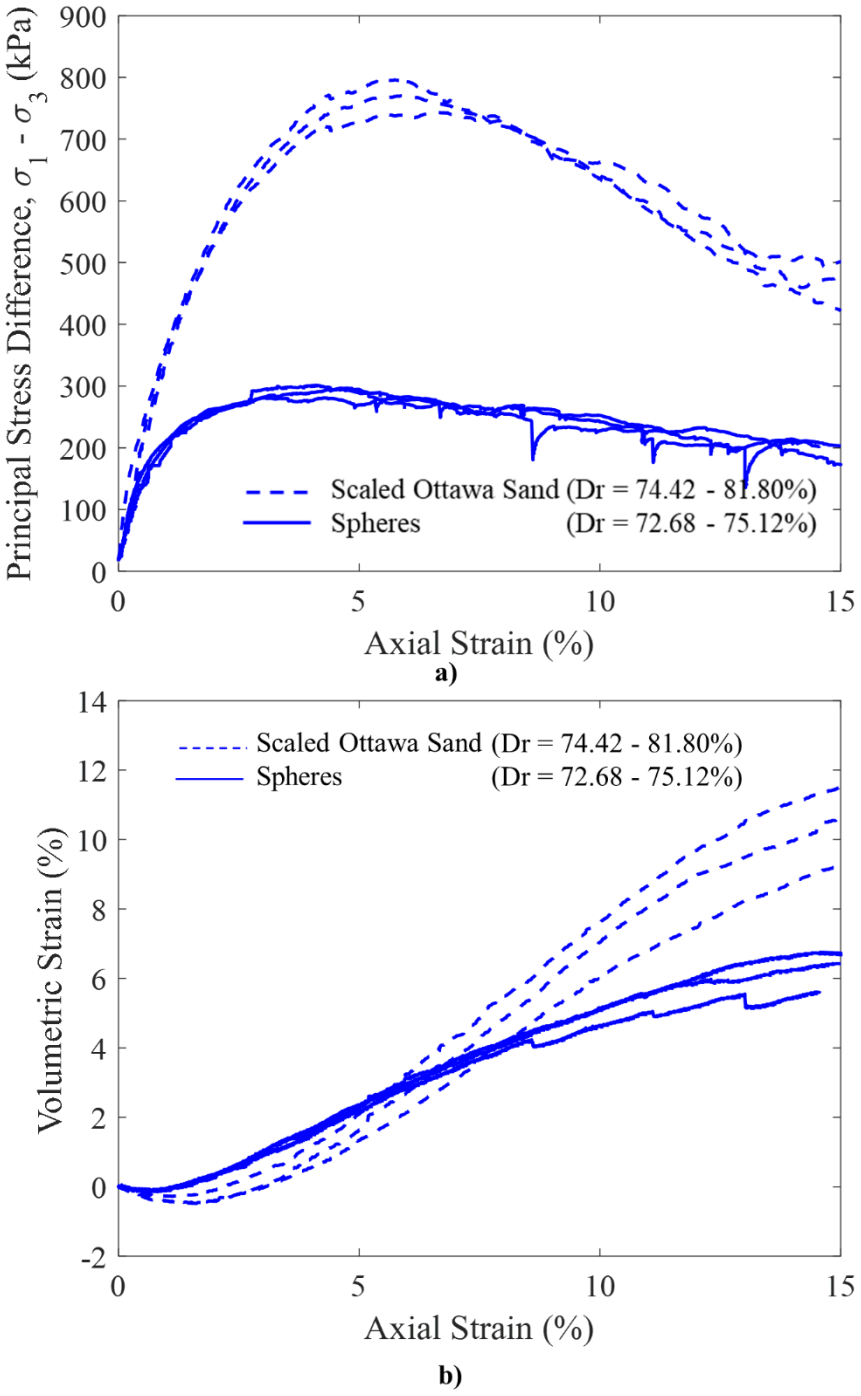

Figure 16: Triaxial shear behavior of scaled Ottawa sand and spheres with medium (10.16 cm diameter): a) principal stress difference b) volumetric strain.

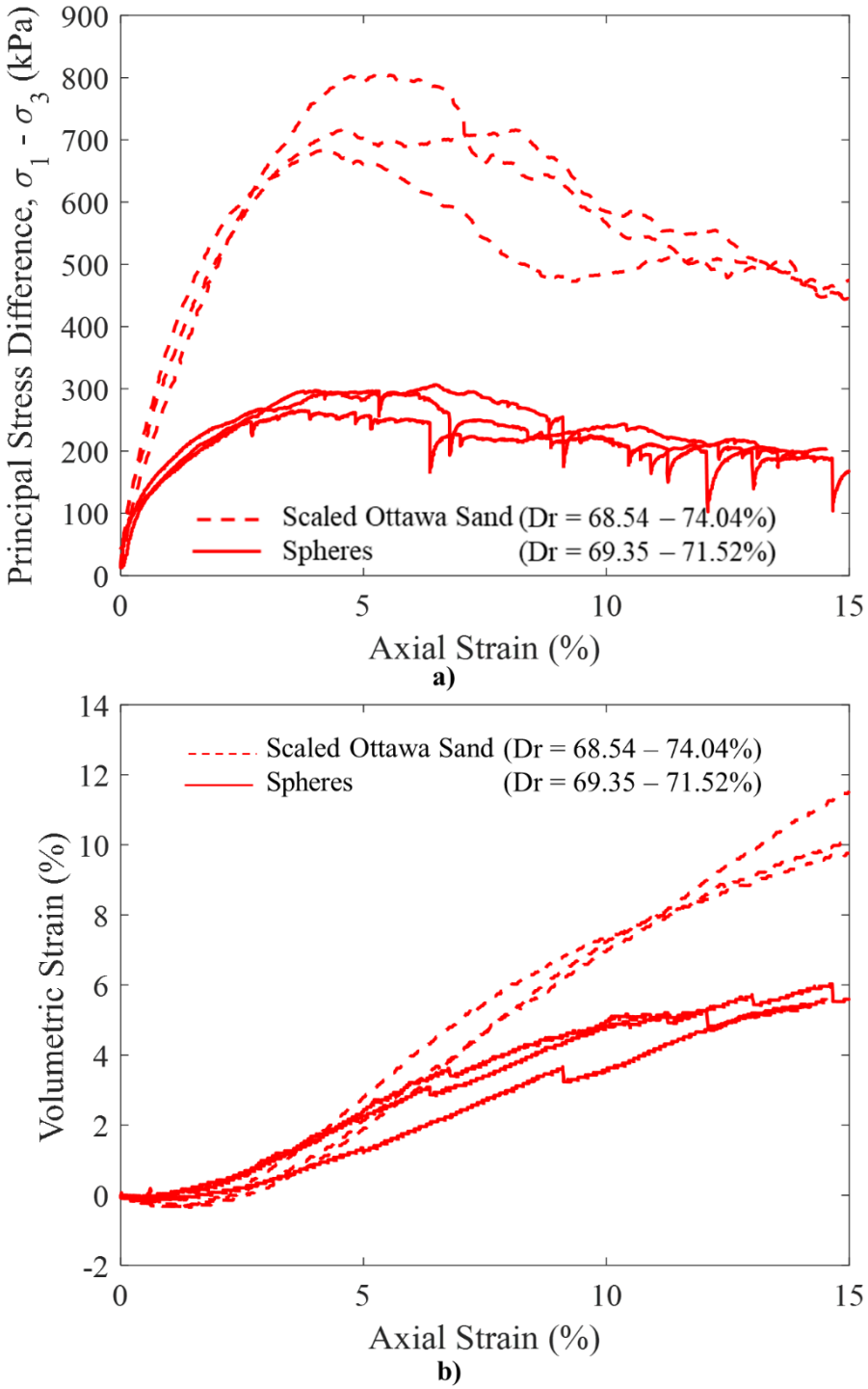

Figure 17: Triaxial shear behavior of scaled Ottawa sand and spheres with small (7.11 cm diameter): a) principal stress difference b) volumetric strain.

Mohr's circles for the 15.24 cm, 10.16 cm, and 7.11 cm specimen with spheres and scaled Ottawa sand can be seen in Figure 18. The relative density, principal effective stress at failure, maximum obliquity at failure, axial strain at failure and friction angle for the 15.24 cm, 10.16 cm, and 7.11 cm diameters can be found in Table 7. The friction angle for both the scaled Ottawa sand and spheres only increase by three degrees from the 15.24 cm diameter to the 7.11 cm diameter test, but the range of friction angles increase as the specimen diameter decreases. On average there is a difference of 15.34° in the friction angle between the scaled Ottawa sand and spheres for each specimen diameter. The Mohr's circles of the spheres are generally in better agreement than the scaled Ottawa sand, but the size effects can be seen for the small specimen with both the spheres and scaled Ottawa sand. Due to the higher relative density of the medium specimen, the scaled Ottawa sand contains the largest major principle stress average. The minor principal stress remains at 100 kPa for the 18 tests due to the consistent confining pressure. When using a specimen diameter to maximum particle diameter ratio between 9:1 to 13:1, the difference in strength parameters was due to relative density. Based on the relationship of normal stress, shear stress, and friction angle with the particle shape and specimen size, it is suggested that the REV is met for the medium and large specimen diameters of the spheres, but slightly violated the REV for the small specimen. The REV is met for the medium and large diameters of the scaled Ottawa sand, but does not reach the minimum REV for the 7.11 specimen.

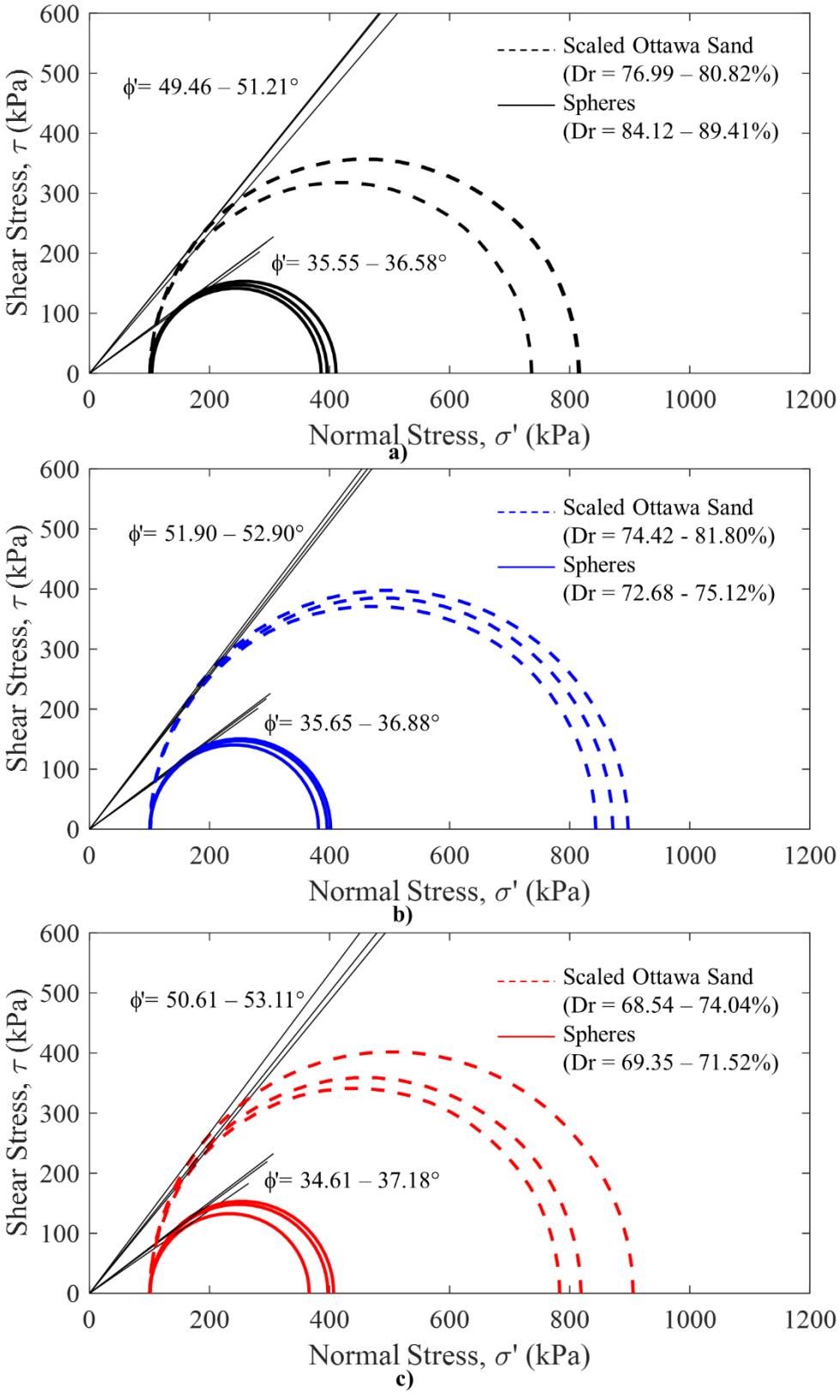

Figure 18: Mohr's circle for scaled Ottawa sand and spheres: a) large specimen b) medium specimen c) small specimen.

Table 7: Test Results for Large, Medium, and Small Specimen.

D (cm)	Shape	Dr (%)	$\sigma'_{1,f} - \sigma'_{3,f}$ (kPa)	$\sigma'_{1,f}/\sigma'_{3,f}$	$\varepsilon_{a,f}$ (%)	ϕ'(°)	ϕ'_{avg}(°)	$\phi'_{max} - \phi'_{min}$(°)
15.32	Sphere	89.41	306.76	3.95	4.58	36.58		
15.29	Sphere	85.29	283.75	3.78	3.15	35.55	36.22	1.03
15.32	Sphere	84.12	295.60	3.94	3.42	36.52		
15.29	Ottawa	78.36	714.33	8.00	5.20	51.07		
15.28	Ottawa	76.99	636.20	7.33	6.24	49.46	50.58	1.75
15.28	Ottawa	80.82	713.92	8.07	5.66	51.21		
10.32	Sphere	72.68	294.92	3.92	4.56	36.40		
10.34	Sphere	75.61	281.04	3.79	3.01	35.65	36.31	1.23
10.36	Sphere	75.12	301.35	4.00	4.10	36.88		
10.34	Ottawa	81.80	796.32	8.88	5.73	52.90		
10.30	Ottawa	74.42	742.95	8.39	6.62	51.90	52.38	1.00
10.34	Ottawa	79.83	770.55	8.59	5.88	52.33		
7.48	Sphere	69.35	265.25	3.63	3.79	34.61		
7.47	Sphere	69.97	306.58	4.06	6.49	37.18	36.11	2.57
7.47	Sphere	71.52	296.54	3.94	5.25	36.53		
7.50	Ottawa	68.54	683.09	7.80	4.14	50.61		
7.49	Ottawa	71.40	718.63	8.16	4.62	51.41	51.71	2.50
7.53	Ottawa	74.04	805.06	8.99	5.55	53.11		

CONCLUSION

The purpose of this research was to investigate the size effects in triaxial testing with the utilization of 3D printed analogue materials so that the influence of shape on REV could be examined without changes in mineralogy, gradation, particle size, or surface properties. Although, there are multiple factors which can cause size effects and dictate the particle diameter to specimen diameter ratio in granular testing, the results were analyzed to see in the minimum REV was met for the 18 triaxial tests based on strength and volumetric behavior. Three specimen diameters were tested (15.24 cm, 10.16 cm, and 7.11 cm) giving specimen diameter to maximum particle size ratios of 13:1, 9:1, and 6:1. Corrections were made for temperature,

membrane penetration, membrane resistance, frictional force of water, the cross sectional area after shearing, and water volume from the piston.

As expected, there was an observable difference in the shearing behavior of the large, medium, and small specimen with spheres and scaled Ottawa sand. When comparing soil response of spheres and scaled Ottawa sand:

1. The friction angle for scaled Ottawa sand was on average 15.34° larger than for spheres.
2. The scaled Ottawa sand had a much higher average maximum principal stress difference of 731.23 kPa as compared to 292.42 kPa
3. The scaled Ottawa sand had a greater amount of dilation and a faster rate of strain softening than the spheres.

When investigating the REV of specimen with different diameter sizes:

1. The variability of principle stress difference and friction angle increased as the specimen diameter decreased.
2. The REV was met for the medium and large specimen when using spheres and scaled Ottawa sand with the difference in strength parameters due to the difference in relative density.
3. The REV was not met for the small specimen due to the variability in strength parameters.

From the results, it is determined that the REV was met for the spheres and the size effects were minimal, although it is likely that the smallest specimen size of 7.11 cm slightly violates the REV and should be avoided if possible. The scaled Ottawa sand and spheres had a

greater increase in variability as the diameter decreases, implying that the REV was not met for the 7.11 cm specimen diameter. Therefore, it is recommended that a minimum specimen diameter should be at least nine time greater than the maximum particle diameter for spheres and subrounded particles in consolidated drained triaxial testing in order to minimize size effects. A future extension of this research project could include the investigation of REV as a function of particle angularity with the addition of 3D printed Toyoura and Hostun sand.

REFERENCES

ASTM D-2435. (2011). Standard Test Methods for One-Dimensional Consolidation Properties of Soils Using Incremental Loading. Philadelphia, PA: ASTM.

ASTM D-4253. (2016). Standard Test Methods for Maximum Index Density and Unit Weight of Soils Using a Vibratory Table. Philadelphia, PA: ASTM.

ASTM D-4254. (2016). Standard Test Methods for Minimum Index Density and Unit Weight of Soils and Calculation of Relative Density. Philadelphia, PA: ASTM.

ASTM D-7181. (2011). Standard Test Method for Consolidated Drained Triaxial Compression Test for Soils. Philadelphia, PA: ASTM.

Baldi, G., & Nova, R. (1984). Membrane penetration effects in triaxial testing. *Journal of Geotechnical engineering*, *110*(3), 403-420.

Bear, J. (1972). Dynamics of fluids in porous media. *American Elsevier Publishing Company*, 10-30.

Bolton, M. D. (1986). The strength and dilatancy of sands. *Geotechnique*, *36*(1), 65-78.

Borges, J. A., Pires, L. F., Cássaro, F. A., Roque, W. L., Heck, R. J., Rosa, J. A., & Wolf, F. G. (2018). X-ray microtomography analysis of representative elementary volume (REV) of soil morphological and geometrical properties. *Soil and Tillage Research*, *182*, 112-122.

BS EN 1997-2: 2007. Eurocode 7—Geotechnical design—Part 2: Ground Investigation and testing.

Cavarretta, I., Coop, M., & O'Sullivan, C. (2010). The influence of particle characteristics on the behaviour of coarse grained soils. *Geotechnique*, *60*(6), 413-423.

Chan, L. C., & Page, N. W. (1997). Particle fractal and load effects on internal friction in powders. *Powder Technology*, *90*(3), 259-266.

Cho, G. C., Dodds, J., & Santamarina, J. C. (2007). Closure to "Particle Shape Effects on Packing Density, Stiffness, and Strength: Natural and Crushed Sands" by Gye-Chun Cho, Jake Dodds, and J. Carlos Santamarina. *Journal of geotechnical and geoenvironmental engineering*, *133*(11), 1474-1474.

Costanza-Robinson, M. S., Estabrook, B. D., & Fouhey, D. F. (2011). Representative elementary volume estimation for porosity, moisture saturation, and air-water interfacial areas in unsaturated porous media: Data quality implications. *Water Resources Research*, *47*(7).

Excel (2016). Microsoft Corporation. *Redmond, WA.*

Fagnoul, A., and Bonnechere, F. (1969). “Shear strength of porphyry materials.” Proc., 7th Int. Conf. on Soil Mechanics and Foundation Engineering, Sociedad Mexicana de Mecanica, Mexico City, 61–65.

Frossard, E. (2006). A new energy approach in granular media mechanics: applications to rockfill dams. Proc. 22nd Int. Congress on Large Dams, Barcelona 5, 191–208.

Frossard, E. (2009). On the structural safety of large rockfill dams. Proc. 23rd Int. Congress on Large Dams, Brasilia, Q.91–R.39 (CD-ROM).

Frossard, É., Hu, W., Dano, C., & Hicher, P. Y. (2012). Rockfill shear strength evaluation: a rational method based on size effects. *Géotechnique*, *62*(5), 415-427.

Frydman, S., Zeitlen, J. G., & Alpan, I. (1973). The membrane effect in triaxial testing of granular soils. *Journal of Testing and Evaluation*, *1*(1), 37-41.

Gitman, I. M., Gitman, M. B., & Askes, H. (2006). Quantification of stochastically stable representative volumes for random heterogeneous materials. *Archive of Applied Mechanics*, *75*(2-3), 79-92.

Holtz, R. D., Kovacs, & W. D., Sheahan, T. C. (2011) An introduction to geotechnical engineering (2nd edition). Upper Saddle River, NJ: *Pearson Eductaion Inc.*

Holtz, W. G., & Gibbs, H. J. (1956). Triaxial shear tests on pervious gravelly soils. *Journal of the Soil Mechanics and Foundations Division*, *82*(1), 1-22.

Hu, W., Merliot, E., Derkx, F., Le Touzo, J. Y., Hicher, P. Y., & Dano, C. (2011). Effect of sample size on the behavior of granular materials. *Geotechnical Testing Journal*, *34*(3), 186-197.

Jones, F. E., & Harris, G. L. (1992). ITS-90 density of water formulation for volumetric standards calibration. *Journal of research of the National Institute of Standards and Technology*, *97*(3), 335.

Kell, G. S., & Whalley, E. (1975). Reanalysis of the density of liquid water in the range 0–150 C and 0–1 kbar. *The Journal of Chemical Physics*, *62*(9), 3496-3503.

LabVIEW (2014). National Instruments. *Austin, TX*.

Marachi, N.D. Chan C.K and Seed H.B. (1972). Evaluation of Properties of Rockfill Materials. *J. of SMFE*, ASCE, 98, SM1, 95-114.

Marachi, N.D., Chan, C.K, Seed, H.B. and Duncan, J.M. (1969). Strength and Deformation Characteristics of Rockfill Materials. Report No. TE 69-5, Civil Eng. Dept., Univ. of California, Berkeley, California, USA.

Marsal, R. J. (1972). Mechanical properties of rockfill: In Embankment dam engineering. Textbook. Eds. RC Hirschfeld and SJ Poulos. JOHN WILEY AND SONS INC., PUB., NY, 1973, 92P.

Marsal, RJ. (1967). Large Scale Testing of Rockfill Materials. *J. of Soil Mech. and Foundations Division*, ASCE, 93(2), 27-43.

Masson, S., & Martinez, J. (2000). Effect of particle mechanical properties on silo flow and stresses from distinct element simulations. *Powder Technology*, *109*(1-3), 164-178.

MATLAB (2017). MathWorks, Inc., *Natick, MA*.

Nitchiporovitch, A. A. (1969). "Shearing strength of coarse shell materials." Proc., 7th Int. Conf. on Soil Mechanics and Foundation Engineering, International Society for Soil Mechanics and Geotechnical Engineering, London, 211–216.

Omar, T., & Sadrekarimi, A. (2014). Specimen size effects on behavior of loose sand in triaxial compression tests. *Canadian Geotechnical Journal*, *52*(6), 732-746.

Omar, T., & Sadrekarimi, A. (2015). Effect of triaxial specimen size on engineering design and analysis. *International Journal of Geo-Engineering*, *6*(1), 5.

Ozelim, L. C. D. S., & Cavalcante, A. L. (2017). Representative Elementary Volume Determination for Permeability and Porosity Using Numerical Three-Dimensional Experiments in Microtomography Data. *International Journal of Geomechanics*, *18*(2), 04017154.

Parafiniuk, P., Molenda, M., & Horabik, J. (2014). Influence of particle shape and sample width on uniaxial compression of assembly of prolate spheroids examined by discrete element method. *Physica A: Statistical Mechanics and its Applications*, *416*, 279-289.

Procter, D. C., & Barton, R. R. (1974). Measurements of the angle of interparticle friction. *Geotechnique*, *24*(4), 581-604.

Razavi, M. R., Muhunthan, B., & Al Hattamleh, O. (2006). Representative elementary volume analysis of sands using X-ray computed tomography. *Geotechnical Testing Journal*, *30*(3), 212-219.

Steinbach, J. (1967), Volume changes due to membrane penetration in triaxial tests on granular materials, M.Sc. Thesis, Cornell University, New York, USA.

Watters, M. and Bernhardt, M. (2017). Modified curing protocol for improved strength of binder-jetted 3D parts, *Rapid Prototyping Journal*, 24(2).

Wei, H., Frossard, E., Hicher, P. Y., & Dano, C. (2010). Method to Evaluate the Shear Strength of Granular Material with Large Particles. *Soil Behavior and Geo-Micromechanics*, 247-254.

Welcher, R. (2004), Effect of fines on the shear strength of unbound aggregate base course, M.Sc. Thesis, University of Arkansas, Arkansas, USA.

Wiącek, J., & Molenda, M. (2016). Representative elementary volume analysis of polydisperse granular packings using discrete element method. *Particuology*, *27*, 88-94.

Wiącek, J., Molenda, M., Ooi, J. Y., & Favier, J. (2012). Experimental and numerical determination of representative elementary volume for granular plant materials. *Granular Matter*, *14*(4), 449-456.

Zhang, H. and Garga, V.K. (1997). Quasi-steady state: A real behavior. *Canadian Geotechnical Journal*, 34, 749-761.